Bi-frequency illumination: a quantum-enhanced protocol

Mateo Casariego,[1,2,*] Yasser Omar,[1,2,†] and Mikel Sanz[3,4,5,‡]

[1]*Physics of Information and Quantum Technologies Group, Instituto de Telecomunicações, Portugal*
[2]*Instituto Superior Técnico, Universidade de Lisboa, Portugal*
[3]*Department of Physical Chemistry, University of the Basque Country UPV/EHU, Apartado 644, E-48080 Bilbao, Spain*
[4]*IQM, Nymphenburgerstr. 86, 80636 Munich, Germany*
[5]*IKERBASQUE, Basque Foundation for Science, Plaza Euskadi 5, 48009 Bilbao, Spain*

We propose a quantum-enhanced sensing protocol to measure the response of a target object to the frequency of a probe in a noisy and lossy scenario. In our protocol, a bi-frequency state illuminates a target embedded in a thermal bath, whose reflectivity $\eta(\omega)$ is frequency-dependent. After a lossy interaction with the object, we estimate the parameter $\lambda = \eta(\omega_2) - \eta(\omega_1)$ in the reflected beam, which captures information about the response of the object to different electromagnetic frequencies. Computing the quantum Fisher information H relative to the parameter λ in an assumed neighborhood of $\lambda \sim 0$ for a two-mode squeezed state (H_Q), and a coherent state (H_C), we show that a quantum enhancement in the estimation of λ is obtained when $H_Q/H_C > 1$. This quantum advantage grows with the mean reflectivity of the probed object, and is noise-resilient. We derive explicit formulas for the optimal observables, and propose a general experimental scheme based on elementary quantum optical transformations. Furthermore, our work opens the way to applications in both radar and medical imaging, in particular in the microwave domain.

Introduction. Quantum information technologies are opening very promising prospects for faster computation, securer communications, and more precise detection and measuring systems, surpassing the capabilities and limits of classical information technologies [1–5]. Namely, in the domain of quantum sensing and metrology [6], we are currently witnessing a boost of applications to a wide spectrum of physical problems: from gravimetry and geodesy [7–11], clock synchronisation [5, 12], thermometry [13] and bio-sensors [14–17], to experimental proposals to seek quantum behavior in macroscopic gravity [18], to name just a few. Most of these studies are focused on unlossy (unitary) scenarios, while the more realistic, lossy case needs to be investigated further [19–22]. It is thus important to propose new sensing protocols that show a quantum enhancement even in the presence of information losses. Quantum illumination [23–32] is a particularly interesting example of a lossy protocol where the use of entanglement proves useful even in an entanglement-braking scenario. In a radar setting, the detection of a low-reflectivity object in a noisy thermal environment with a low-intensity signal is shown to be enhanced when the signal is entangled to an idler that is kept for a future joint measurement with the reflected state. The decision problem of whether there is an object or not can be rephrased as a quantum estimation of the object's reflectivity η, in order to discriminate an absence ($\eta = 0$) from a presence ($\eta \ll 1$) of a low-reflectivity object [3].

The goal of quantum estimation [34] is to construct an estimator $\tilde{\lambda}$ for certain parameter λ characterizing the system. It is noteworthy that not every parameter in a system corresponds to an observable, which may imply data post-processing. However, the theory provides techniques to obtain an optimal observable –not necessarily unique, *i.e.* whose mean square error is minimal. The estimator $\tilde{\lambda}$ is nothing but a map from the results of measuring the optimal observable to the set of possible values of the parameter λ. One of the main results of this theory is the quantum Cramér-Rao (qCR) bound, which sets the ultimate precision of any estimator. Whether this bound is achievable or not depends on the data-analysis method used, and on the nature of the experimental noise. In most practical situations, maximum likelihood methods for unbiased estimators, together with Gaussian noise make the bound achievable. In order to find the qCR – and the explicit form of the optimal observable– one needs to compute the quantum Fisher information [35] (QFI), which roughly speaking quantifies how much information about λ can be extracted from the system, provided that an optimal measurement is performed. In general, computing the QFI involves diagonalisation of the density matrix, which makes the obtention of analytical results challenging. However, if one restricts to Gaussian states and Gaussian-preserving operations, the so-called symplectic approach simplifies the task considerably [36]. As the QFI is by definition optimized over all POVMs, it only depends on the initial state, often called *probe*. This means that a second optimization of the QFI can be pursued, this time over all possible probes. Moreover, this approach allows us to quantitatively compare different protocols, *e.g.* with and without entanglement in the probe, since an increase in the QFI when the same resources are used – which typically translates into fixing the particle number or the energy– directly means an improvement in precision.

Here, we propose a quantum-enhanced, lossy protocol to decide whether an object embedded in a noisy environment has a frequency-dependent reflectivity or not. In a radar-like setting, this can be seen as a second step after quantum illumination: once the detection is completed, we may be interested in extracting further information about the object, *e.g.* whether it is sensitive to frequency changes in the light it is illuminated with. In the Supplemental Material [37] we test our methods to reproduce the results of quantum illumination. The protocol comprises: a bi-frequency state sent to probe a target, which is modeled as a beam splitter with a frequency-dependent reflectivity $\eta(\omega)$. The object is embed-

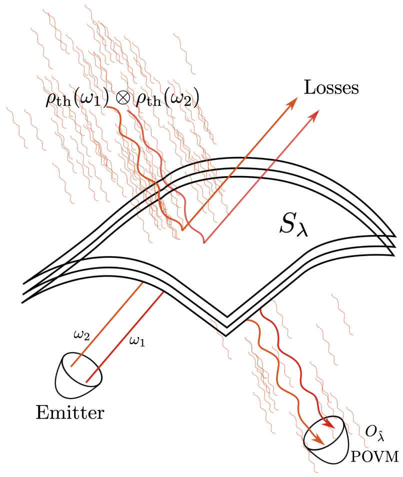

FIG. 1. An object reflects a bi-frequency beam (notice the similar colors of the two beams coming out of the emitter), and mixes it with a thermal bath, coming from the upper left. The transmitted signal and reflected thermal state are lost, and a measurement $O_{\hat{\lambda}}$ is performed onto the available part (lower right corner), whose expectation values converge, after classical data processing, to an estimator of the parameter λ encoded in the object. In our case, S_λ represents a multi-layered object acting as a beam splitter, and $\lambda := \eta_2 - \eta_1$, where $\eta_i = \eta(\omega_i)$ are the reflectivities for the different frequencies. The emitter can in principle entangle the two modes, which proves advantageous in the parameter estimation.

ded in a noisy environment, which is assumed to be in a thermal state with equal expected photon number for both frequencies ω_1 and ω_2, a good approximation provided that we assume a short frequency distance. The goal is to obtain an estimator for the parameter $\lambda = \eta(\omega_2) - \eta(\omega_1)$, that captures information about the frequency dependence of the beam splitter. It is assumed that the frequencies are sufficiently close so that we can work in a neighborhood of $\lambda \sim 0$. This is not only a useful approach within estimation theory, but also a requirement when we assumed that the two thermal baths contain the same number of photons. For a more detailed and quantitative discussion, see the Supplemental Material [37]. By imposing that the expected photon number is the same in quantum and classical scenarios, we find the QFI ratio between them, and analyze when it is greater than one. We find that the maximum advantage is obtained for highly reflective targets, and derive explicit limits in the highly noisy case. We also provide expressions for the optimal observables, proposing a general experimental scheme described in FIG. S2 of the Supplemental Material [37], and motivating applications in microwave technology [38].

Model, and fundamentals of quantum estimation theory. The model is synthesized in FIG. 1: the target object, modeled as a beam splitter with a frequency-dependent reflectivity is subject to an illumination with a bi-frequency probe. For a single frequency, a beam splitter is characterised by a unitary operator $U(\omega) \equiv \exp\left[\arcsin\left(\sqrt{\eta(\omega)}\right)(\hat{s}^\dagger_\omega \hat{b}_\omega e^{i\varphi} - \hat{s}_\omega \hat{b}^\dagger_\omega e^{-i\varphi})\right]$, where $\eta(\omega)$ is a frequency-dependent reflectivity, related to transmittivity τ via $\eta(\omega) + \tau(\omega) = 1$. We assume for simplicity that $\varphi = 0$, *i.e.* there is no phase difference between transmitted and reflected signals. This unitary maps states (density matrices) that live in the density matrix space associated with Hilbert space $\mathcal{H}$, $\mathcal{D}(\mathcal{H})$ to itself. Formulating the problem from a density operator perspective, we have that the received state is $\rho_\lambda = \mathrm{Tr}_{S_1}\mathrm{Tr}_{S_2}\left[U_\lambda \rho U_\lambda^\dagger\right]$, where $\rho \in \mathcal{H}_{S_1,S_2,B_1,B_2}$ is a four-mode state that includes the two signals (the two-mode state that we can control) and two thermal environments of the form $\rho_1^{th} \otimes \rho_2^{th}$, where the subscript indicates the frequency, *i.e.* $\rho_a^{th} = (1+N_{\rm th})^{-1}\sum_{n=0}^\infty (N_{\rm th}/(1+N_{\rm th}))^n |n\rangle_a \langle n|$ where $N_{\rm th} = \mathrm{Tr}(\rho_a^{th}\hat{b}^\dagger_{\omega_a}\hat{b}_{\omega_a})$ is the average number of thermal photons, which we assume to be the same for the two modes. This assumption is accurate for sufficiently small frequency difference $\omega_1 - \omega_2$ [37]. The interaction U_λ comes from reparametrizing the four-mode unitary $U(\omega_1)\otimes U(\omega_2)$ using the difference of reflectivities $\lambda \equiv \eta_2 - \eta_1$.

The quantum Fisher information $H(\lambda)$ quantifies the information about the value of λ that can be extracted from a state ρ_λ. It assumes that an optimal measurement is performed. The usual basis-dependent expression for the QFI is:

$$H(\lambda) = 2\sum_{m,n}\frac{|\langle\Phi_m|\,\partial_\lambda\rho_\lambda\,|\Phi_n\rangle|^2}{\rho_m+\rho_n}, \tag{1}$$

where $\{|\Phi_m\rangle, \rho_m\}_m$ are the solutions to the eigenproblem of ρ_λ. Regardless of the basis one uses –the Fock number basis or a coherent representation of states– the problem becomes hard to solve analytically. However, in the framework of Gaussian states the calculation becomes simpler. Gaussian states have a very convenient phase-space representation: they can be fully characterised by their first and second moments: the displacement vector $\vec{d}$ and the covariance matrix Σ, respectively. The QFI of a λ-parametrised Gaussian state $(\Sigma_\lambda, \vec{d})$ can be computed as

$$\begin{aligned} H(\lambda) = \frac{1}{2(\det[A]-1)}&\Big[\det[A]\,\mathrm{Tr}\left[(A^{-1}\dot{A})^2\right] \\ &+ \sqrt{\det[\mathbb{1}_2 + A^2]}\,\mathrm{Tr}\left[\left((\mathbb{1}_2+A^2)^{-1}\right)^2\right] \\ &- f(\nu_+,\nu_-)\Big] + 2\dot{\vec{d}}^\dagger \mathbf{\Sigma}^{-1}\dot{\vec{d}}, \end{aligned} \tag{2}$$

where $f(\nu_+,\nu_-) := 4\left(\nu_+^2 - \nu_-^2\right)\left(\frac{(\partial_\lambda\nu_+)^2}{\nu_+^4-1} - \frac{(\partial_\lambda\nu_-)^2}{\nu_-^4-1}\right)$, the *dot* over A and $\vec{d}$ denotes derivative with respect to λ, and $\nu_\pm$ are the *symplectic eigenvalues* of Σ_λ, defined as following Ref. [2]

$$2\nu_\pm^2 := \mathrm{Tr}[A^2] \pm \sqrt{(\mathrm{Tr}[A^2])^2 - 16\det[A]}, \tag{3}$$

with the matrix A given by $A := i\Omega T \Sigma_\lambda T^\intercal$, $\Omega := \mathrm{antidiag}(\mathbb{1}_2, -\mathbb{1}_2)$, and $T_{ij} := \delta_{j+4,2i} + \delta_{j,2i-1}$ is the matrix that changes the basis to the *quadrature basis* $(\hat{x}_1^{\rm th}, \hat{x}_1^{\rm S}, \hat{x}_2^{\rm th}, \hat{x}_2^{\rm S}, \hat{p}_1^{\rm th}, \hat{p}_1^{\rm S}, \hat{p}_2^{\rm th}, \hat{p}_2^{\rm S})^\intercal$. As mentioned above, this value of the QFI is obtained when an optimal measurement is performed. In Ref. [34] and references therein it was proven that the qCR bound is saturated by

$$\hat{O}_\lambda = \lambda \mathbb{1} + \hat{L}_\lambda / H(\lambda), \tag{4}$$

where $\mathbb{1}$ is the identity operator and $\hat{L}_\lambda$ is a symmetric logarithmic derivative (SLD) fulfilling the equation $\{\hat{L}_\lambda, \rho_\lambda\} = 2\partial_\lambda \rho_\lambda$, where $\{\cdot,\cdot\}$ denotes the anticommutator. Assuming that the estimator $\tilde{\lambda}$ is constructed using maximum likelihood methods so that the qCR bound is asymptotically achieved, the optimal observable is the one with the lowest possible variance, saturating the qCR inequality and yielding an optimal estimator after classically processing the measurement outcomes. For a Gaussian state $\left(\Sigma_\lambda, \vec{d}_\lambda\right)$ written in the complex basis, the symmetric logarithmic derivative given in Ref. [36] is

$$\hat{L}_\lambda = \Delta\vec{\hat{A}}^\dagger \mathcal{A}_\lambda \Delta\vec{\hat{A}} - \mathrm{Tr}[\Sigma_\lambda \mathcal{A}_\lambda]/2 + 2\Delta\vec{\hat{A}}^\dagger \Sigma_\lambda^{-1} \partial_\lambda \vec{d}_\lambda, \tag{5}$$

where $\Delta\vec{\hat{A}} := \vec{\hat{A}} - \vec{d}_\lambda$, $\vec{\hat{A}}$ the *complex basis* vector of bosonic operators, $\mathcal{A}_\lambda := \mathcal{M}^{-1}\partial_\lambda \vec{d}_\lambda$, where $\mathcal{M} = \bar{\Sigma}_\lambda \otimes \Sigma_\lambda - K \otimes K$, where the bar denotes complex conjugate, and $K := \mathrm{diag}\left(\mathbb{1}_2, -\mathbb{1}_2\right)$. Note that when $\lambda \to 0$ we have $\hat{O}_{\lambda=0} \equiv \hat{O} = \hat{L}_{\lambda=0}/H(\lambda = 0)$, since both limits exist independently. This limit is of our interest because we work in a neighbourhood of $\lambda \sim 0$, *i.e.* the measured value of the parameter is expected to be small. In the next section, we apply the formulas to the case of a two-mode squeezed vacuum state probe.

Two-mode squeezed vacuum state. The TMSV state is the continuous-variable equivalent of the Bell state, being the Gaussian state that optimally transforms classical resources (light, or photons) into quantum correlations. The TMSV state is a cornerstone in experiments with quantum microwaves [40–42]. In our case, we are interested in states produced via nondegenerate parametric amplification, in order to have two distinguishable frequencies. The state can be formally written as: $|\psi\rangle_{\text{TMSV}} := (\cosh r)^{-1} \sum_{n=0}^{\infty} \left(-e^{i\phi}\tanh r\right)^n |n, n\rangle$, where $r \in \mathbb{R}_{\geq 0}$ is the *squeezing parameter* . For simplicity we take $\phi = 0$. The total initial (real) covariance matrix – written in the *real basis* $(\hat{x}_1^{\text{th}}, \hat{p}_1^{\text{th}}, \hat{x}_1^{\text{S}}, \hat{p}_1^{\text{S}}, \hat{x}_2^{\text{th}}, \hat{p}_2^{\text{th}}, \hat{x}_2^{\text{S}}, \hat{p}_2^{\text{S}})^\intercal$– is given by

$$\Sigma = \begin{bmatrix} \Sigma_{\text{th}} & 0 & 0 & 0 \\ 0 & \Sigma_r & 0 & \varepsilon_r \\ 0 & 0 & \Sigma_{\text{th}} & 0 \\ 0 & \varepsilon_r^\intercal & 0 & \Sigma_r \end{bmatrix}, \tag{6}$$

where $\Sigma_{\text{th}} = (1 + 2N_{\text{th}})\mathbb{1}_2$ is the real covariance matrix of a thermal state, $\Sigma_r = \cosh(2r)\mathbb{1}_2$ corresponds to the diagonal part of one of the modes in a TMSV state, and $\varepsilon_r = \sinh(2r)\sigma_Z$ is the correlation between the two modes, where σ_Z is the Z Pauli matrix. We rewrite the covariance matrix in terms of the mean photon number $N_{\text{S}} \equiv \langle \hat{a}_{S_1}^\dagger \hat{a}_{S_1}\rangle = \langle \hat{a}_{S_2}^\dagger \hat{a}_{S_2}\rangle$, using the relation $\sqrt{N_{\text{S}}} = \sinh r$ [43]. This gives $\sinh(2r) = 2\sqrt{2N_{\text{S}}(1 + 2N_{\text{S}})}$ and $\cosh(2r) = 1 + 4N_{\text{S}}$. The displacement vector of a TMSV state is identically zero $\vec{d}_{\text{TMSV}} = \vec{0}$, so the last term of Eq. (2) vanishes. Under the assumption that the object does not entangle the two modes, we have that the symplectic transformation is $S(\eta_1, \eta_2) = S_{\text{BS}}(\eta_1) \oplus S_{\text{BS}}(\eta_2)$ [44], where

$$S_{\text{BS}}(x) = \begin{bmatrix} \sqrt{x}\mathbb{1}_2 & \sqrt{1-x}\mathbb{1}_2 \\ -\sqrt{1-x}\mathbb{1}_2 & \sqrt{x}\mathbb{1}_2 \end{bmatrix} \tag{7}$$

is the real symplectic transformation associated with a beam splitter of reflectivity x. We define the parameter of interest as $\lambda \equiv \eta_2 - \eta_1$. With this, $S(\eta_1, \eta_2)$ becomes a function of λ. For simplicity, we define $S_\lambda := S(\eta_1, \eta_1 + \lambda)$. The full state after the signals get mixed with the thermal noise is given by $\tilde{\Sigma}_\lambda \equiv S_\lambda \Sigma S_\lambda^\intercal$. In covariance matrix formalism, partial traces are implemented by removing the corresponding rows and columns [1]; in our case the rows and columns 1, 2, 5, and 6. The resulting *received* covariance matrix reads as follows

$$\Sigma_\lambda = \begin{bmatrix} a\mathbb{1} & b\sigma_Z \\ b\sigma_Z & c_\lambda \mathbb{1} \end{bmatrix}, \tag{8}$$

with $a \equiv 1 + 2N_{\text{th}} + 2\eta_1(2N_{\text{S}} - N_{\text{th}})$, $b \equiv 2\sqrt{2}\sqrt{\eta_1}\sqrt{N_{\text{S}}(2N_{\text{S}}+1)}\sqrt{\eta_1 + \lambda}$, and $c_\lambda \equiv 1 + 2N_{\text{th}} + 2(\eta_1 + \lambda)(2N_{\text{S}} - N_{\text{th}})$. For this state, the symplectic eigenvalues $\nu_\pm$ defined in Eq. (3) are strictly larger than one for any value of the parameters N_{S}, N_{th} and η_1, so there is no need of any regularization scheme [2]. In what follows, we work in a neighborhood of $\lambda \sim 0$ – which can be implemented by taking the limit $\lambda \to 0$ in the derived expressions. This is a physical assumption, since we are interested in probing regions of $\eta(\omega)$ that do not change drastically, *i.e.* that are well approximated by a linear function with either no slope or a small one. We obtain the function $H_Q = H_Q(\eta_1, N_{\text{S}}, N_{\text{th}})$ from Eq. (2). An explicit expression can be found in [37]. In the following section, we compute the QFI of a classical probe.

Classical probe. Here we use a pair of coherent states as probe: $|\psi\rangle = |\alpha\rangle \otimes |\alpha\rangle$. The total expected photon number in this state is $2N_{\text{C}} := 2\left|\alpha^2\right|$. For simplicity we take $\alpha \in \mathbb{R}$. The symplectic eigenvalues are always larger than one in this case, so no regularization is required. The initial displacement vector in the real basis is $\vec{d}_0^\intercal = (0, 0, \sqrt{2}\alpha, 0, 0, 0, \sqrt{2}\alpha, 0)$ which leads –after the interaction and the trace of the losses– to $\vec{d}^\intercal = \alpha(\sqrt{2\eta_1}, 0, \sqrt{2(\eta_1 + \lambda)})$. Inserting these in Eq. (2), and taking the limit $\lambda \to 0$, we find that the QFI for the coherent state is

$$H_C = \frac{4N_{\text{th}}^2\left((1 + 2N_{\text{th}}\tau_1)^2 + 1\right)}{(1 + 2N_{\text{th}}\tau_1)^4 - 1} + \frac{N_{\text{S}}}{\eta_1 + 2N_{\text{th}}\tau_1\eta_1}, \tag{9}$$

where $\tau_1 = 1 - \eta_1$ is the transmittivity, and we have set the resources $\left|\alpha^2\right| = N_{\text{S}}$ for a fair comparison with the TMSV state. Having computed both the quantum and the classical QFIs, in the next section we analyse their ratio H_Q/H_C, a quantifier for the quantum enhancement.

Quantum advantage. We analyze the ratio between the TMSV state's QFI (H_Q) and the coherent pair's QFI (H_C) for different situations. Finding values of $(\eta_1, N_{\text{th}}, N_{\text{S}})$ such that the ratio H_Q/H_C is larger than one means that one can extract more information about parameter λ using a TMSV than using a coherent pair, provided an optimal measurement is performed in both cases. We plot the results for various values of η_1 (see FIG. 2). We can immediately see that the ratio gets larger for large values of η_1, *i.e.* for highly reflective materials. In particular, we find the high-reflectivity limit:

$$\lim_{\eta_1\to 1}\frac{H_{\text{Q}}}{H_{\text{C}}}=\frac{N_{\text{S}}^2\left(8N_{\text{th}}(N_{\text{th}}+1)+4\right)+4N_{\text{S}}N_{\text{th}}^2+N_{\text{th}}^2}{N_{\text{th}}\left(N_{\text{S}}(4N_{\text{th}}+2)+N_{\text{th}}\right)} \tag{10}$$

which converges to $1+8N_{\text{S}}^2/(4N_{\text{S}}+1)$ in the highly noisy scenario $N_{\text{th}}\gg 1$. In the next sections we explicitly compute the observables that lead to an optimal extraction of λ's value for both the classical and the quantum probes.

Optimal observable for the TMSV state probe. Computing the SLD in Eq. (2) and inserting it in Eq. (4) we find $\hat{O}_Q = L_{11}\hat{a}_1^\dagger\hat{a}_1 + L_{22}\hat{a}_2^\dagger\hat{a}_2 + L_{12}\left(\hat{a}_1^\dagger\hat{a}_2^\dagger + \hat{a}_1\hat{a}_2\right) + L_0\mathbb{1}_{12}$, where the general expressions for the coefficients can be found in [37]. Here we focus on the high-reflectivity target, where the maximum quantum enhancement is expected. Moreover, it is illustrative to study the noiseless case, since this captures the essence of what is being measured:

$$\begin{aligned}\lim_{\substack{N_{\text{th}}\to 0\\ \eta_1\to 1}}\hat{O}_Q &= -\mu^2\hat{a}_1^\dagger\hat{a}_1 - \hat{a}_2^\dagger\hat{a}_2\\ &\quad+\mu\left(\hat{a}_1^\dagger\hat{a}_2^\dagger+\hat{a}_1\hat{a}_2\right)-\nu\mathbb{1}_{12},\end{aligned} \tag{11}$$

where $\mu^2 \equiv (1+1/2N_{\text{S}})$ and $\nu \equiv (1+1/4N_{\text{S}})$. We can rewrite this observable as $\hat{b}^\dagger\hat{b}-1$, *i.e.* implementing photon-counting on the operator $\hat{b} \equiv -i\left(\hat{a}_2^\dagger - \mu\hat{a}_1\right)$. A detailed construction of these operators employing usual resources in superconducting circuit technology, such as Josephson parametric amplifiers [46, 47] is provided in [37].

Optimal observable for the coherent state probe. The optimal observable in this case is given by $\hat{O}_C = 2A\mathbb{1}_{(1)}\otimes\left[\left(\hat{a}_2^\dagger-\eta_1\sqrt{\alpha}\right)\left(\hat{a}_2-\eta_1\sqrt{\alpha}\right)+\frac{1}{2}\right]$, where $A = 1/2(\eta_1 - 1)(1-N_{\text{th}}(\eta_1-1))$ and $\mathbb{1}_{(1)}$ is the absence of active measurement of mode 1. The interpretation is simple: because η_1 is known (it serves as a reference), there is nothing to be gained by measuring the first mode in the absence of entanglement. Moreover, the observable is separable, as one should expect, and the experimental implementation is straightforward: photon-counting in the –locally displaced– second mode. As discussed in the Supplemental Material [37], implementations of these observables in microwave technology implies having both efficient photon-counters [48] and good digital filters [49].

Conclusions. Quantum metrology in the presence of losses is a highly relevant subject for realistic applications, with only a handful of known protocols exhibiting quantum enhancement. Here, we have developed a method for achieving a quantum enhancement in the decision problem of whether a target's reflectivity depends or not on the electromagnetic frequency, using only a bi-frequency, entangled probe, and in the presence of both noise and losses. Such measurement can be used to extract information about the electromagnetic response of a reflective object to changes in frequency, and, consequently, it can be applied to a wide spectrum of situations. It is important to stress that although our results are general and platform-independent, the atmospheric transparency window in the microwaves regime, together with the naturally noisy character of open-air, makes applications in quantum microwaves our first choice [38, 48, 50–53]. Namely, our results could find applications in radar physics, where the protocol could be understood as complementary to quantum illumination: quantum signals can enhance the precision of measurement without increasing the intensity, something very convenient when the emitter does not want to be detected. Entanglement is thus seen as a resource in practical quantum metrology. Moreover, accurate medical imaging with non-ionizing radiation is a permanent goal in medicine. Microwaves, however, when applied in intense ways, can damage the sample. Resorting to methods that increase the precision and/or resolution while keeping a low intensity of radiation is thus crucial for non-invasive imaging technologies. Our results suggest that this quantum advantage will be more significant in the high reflectivity regime, which could prove useful for contrast imaging of tissues with a low penetration depth. The theoretical methods used are not unique to our protocol, and we hope our results can boost efforts in the direction of lossy Gaussian quantum estimation: these are powerful tools that allow us not only to find quantum-enhanced protocols, but also to explicitly find the optimal observables, making the transition to actual experimental proposals quite direct. Using these techniques, we have proved that the scaling of the quantum Fisher information (QFI) when using entanglement is faster than when only classical (coherent) states are used. We have derived analytic expressions for the optimal observables, which are the ones that allow the extraction of the maximum available information of the parameter of interest, constructing an optimal estimator after appropriate classical data processing. Our work paves the way to extensions of the protocol to accommodate both presence of thermal effects in the input modes, and continuous-variable frequency entanglement [54], where a more realistic model for a beam containing a given distribution of frequencies could be used instead of sharp, ideal bi-frequency states.

The authors thank Vahid Salari and Gonçalo Frazão for useful discussions and comments, and acknowledge the support from the EU H2020 Quantum Flagship project QMiCS (820505). MC acknowledges support from the DP-PMI and FCT (Portugal) through scholarship PD/BD/135186/2017. MC and YO thank the support from Fundação para a Ciência e a Tecnologia (Portugal), namely through project UIDB/50008/2020, as well as from project TheBlinQC supported by the EU H2020 QuantERA ERA-NET Cofund in

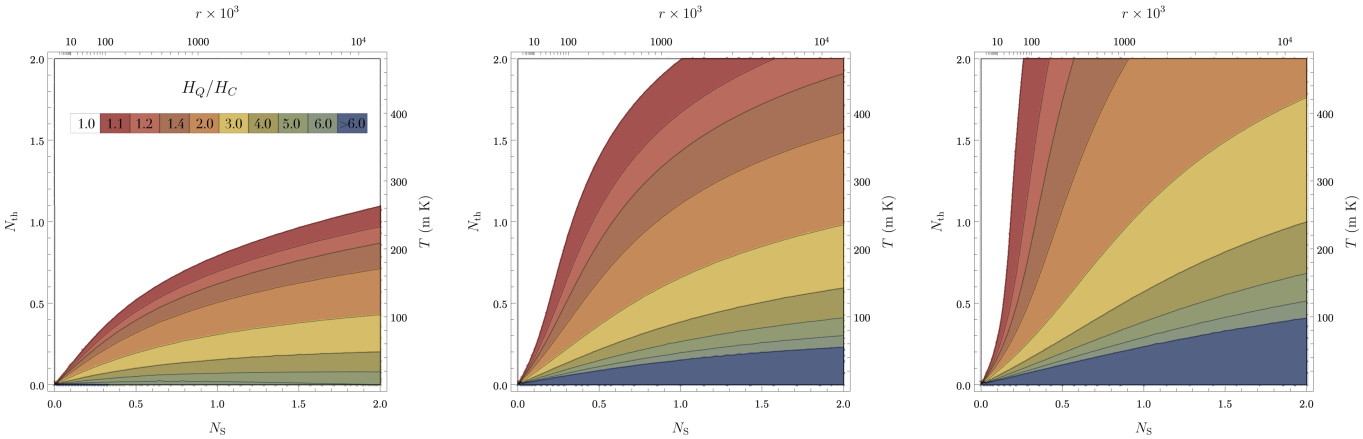

a) $\eta_1 = 0.75$ b) $\eta_1 = 0.90$ c) $\eta_1 = 0.95$

FIG. 2. Values, represented by a non-linear color grading, of the quantum enhancement given by the ratio H_Q/H_C of the quantum Fisher information of the two-mode squeezed vacuum state probe H_Q by the quantum Fisher information of the coherent states probe H_Q as a function of the photon numbers of the signal (N_{S}) and of the thermal bath (N_{th}), for a reflectivity η_1 of a) 0.75, b) 0.90, and c) 0.95. Equivalently, scales of squeezing, r, given by $\sqrt{N_{\mathrm{S}}} = \sinh r$, and temperature T in Kelvin, are provided. The relation between temperature and mean thermal photon number is obtained via the usual Bose-Einstein distribution $N_{\mathrm{th}} = 1/(\exp(E/k_B T) - 1)$ when the energy is set to $E = \hbar\omega = h\nu$, which requires a choice of the frequency ν. We have taken $\nu = 5$ GHz, a typical frequency of microwaves. White represents no quantum enhancement, *i.e.* $H_Q/H_C = 1$. We clearly see that as η_1 grows, the quantum advantage becomes not only more significant, but also easier to achieve with less signal photons. Importantly, as the reference reflectivity η_1 grows, the protocol becomes more resilient to thermal noise. For the full range $\eta_1 \in [0, 1]$ see the Supplemental Material [37].

Quantum Technologies and by FCT (QuantERA/0001/2017). MS thanks support from the Spanish Government PGC2018-095113-B-I00 (MCIU/AEI/FEDER, UE), and Basque Government IT986-16, the project OpenSuperQ (820363) of the EU Flagship on Quantum Technologies, as well as the EU FET Open project Quromorphic (828826). This work is supported by the U.S. Department of Energy, Office of Science, Office of Advanced Scientific Computing Research (ASCR) quantum algorithm teams program, under field work proposal number ERKJ333.

* mateo.casariego@tecnico.ulisboa.pt
† yasser.omar@lx.it.pt
‡ mikel.sanz@ehu.es

[1] M. A. Nielsen and I. L. Chuang. Quantum Computation and Quantum Information: 10th Anniversary Edition. Cambridge University Press, 2010.

[2] F. Arute, J. Arya, R. Babbush, D. Bacon, J. C. Bardin, R. Barends, R. Biswas, S. Boixo, F. G. S. L. Brandao, H. Neven, J. M. Martinis *et al.*. Quantum supremacy using a programmable superconducting processor. Nature, 574(7779):505–510 (2019).

[3] S. L. Braunstein. Quantum limits on precision measurements of phase. Phys. Rev. Lett., **69** 3598–3601 (1992).

[4] S. Pirandola, B. R. Bardhan, T. Gehring, C. Weedbrook, and S. Lloyd. Advances in photonic quantum sensing. Nature Photonics, 12(12):724–733, (2018).

[5] H. Katori, Optical lattice clocks and quantum metrology, Nature Photonics **5**, 203–210 (2011).

[6] V. Giovannetti, S. Lloyd, and L. Maccone. Advances in quantum metrology. Nature Photonics, 5(4):222–229 (2011).

[7] K. Bongs and Y. Singh, Earth-based clocks test general relativity, Nature Photonics **14**, 408–409 (2020).

[8] V. Ménoret, P. Vermeulen, N. Le Moigne, S. Bonvalot, P. Bouyer, A. Landragin, and B. Desruelle, Gravity measurements below 10^{-9} g with a transportable absolute quantum gravimeter, Scientific Reports **8**, 12300 (2018).

[9] J. Flury, Relativistic geodesy, Journal of Physics: Conference Series 723, 012051 (2016).

[10] J. Grotti et al., Geodesy and metrology with a transportable optical clock, Nature Physics **14**, 437–441 (2018).

[11] E. Zeuthen, E. S. Polzik, and F. Ya. Khalili, Gravitational wave detection beyond the standard quantum limit using a negative-mass spin system and virtual rigidity, Phys. Rev. D **100**, 062004 (2019).

[12] Remote quantum clock synchronization without synchronized clocks E. O. Ilo-Okeke, L. Tessler, J. P. Dowling, and T. Byrnes, NPJ: Quantum Information, volume 4, Article number: 40 (2018).

[13] A. De Pasquale, T. M. Stace, Quantum Thermometry (2018). In: F. Binder, L. Correa, C. Gogolin, J. Anders, G. Adesso (eds), *Thermodynamics in the Quantum Regime*. Fundamental Theories of Physics, vol 195. Springer, Cham.

[14] M. H. Mohammady, H. Choi, M. E. Trusheim, A. Bayat, D. Englund, Y. Omar, Low-control and robust quantum refrigerator and applications with electronic spins in diamond, Phys. Rev. A **97**, 042124 (2018).

[15] J. Cai, F. Jelezko, and M. B. Plenio, Hybrid sensors based on colour centres in diamond and piezoactive layers, Nature Communications **5**: 4065 (2014).

[16] F. Dolde et al., Electric-field sensing using single diamond spins, Nature Physics **7**, 459–463 (2011).

[17] K. Jensen et al., Non-invasive detection of animal nerve impulses with an atomic magnetometer operating near quantum limited sensitivity, Scientific Reports **6**, 29638 (2016).

[18] G. Milburn et al., A Spin Entanglement Witness for Quantum Gravity, Phys. Rev. Lett. **119**, 240401 (2017).

[19] S. Lee, Y. S. Ihn, and Z. Kim, Optimal entangled coherent states in lossy quantum-enhanced metrology, Phys. Rev. A **101**, 012332 (2020).

[20] C. Oh, S. Lee, H. Nha, and H. Jeong, Practical resources and measurements for lossy optical quantum metrology, Phys. Rev. A **96**, 062304 (2017).

[21] X. Zhang, Y. Yang, and X. Wang, Lossy quantum-optical metrology with squeezed states, Phys. Rev. A **88**, 013838 (2013).

[22] Y. M. Zhang, X. W. Li, W. Yang, and G. R. Jin, Quantum Fisher information of entangled coherent states in the presence of photon loss, Phys. Rev. A **88**, 043832 (2013).

[23] S. Lloyd, Enhanced Sensitivity of Photodetection via Quantum Illumination, Science **321**, 5895 (2008).

[24] S. Tan, B. I. Erkmen, V. Giovannetti, S. Guha, S. Lloyd, L. Maccone, S. Pirandola, and J. H. Shapiro. Quantum Illumination with Gaussian States. Phys. Rev. Lett. **101**, 253601 (2008).

[25] S. Guha and B. I. Erkmen, Gaussian-state quantum-illumination receivers for target detection, Phys. Rev. A **80**, 052310 (2009)

[26] J. H. Shapiro, The Quantum Illumination Story, IEEE Aerospace and Electronic Systems Magazine, **35**, no. 4, pp. 8-20 (2020).

[27] S. Ray, J. Schneeloch, C. C. Tison, P. M. Alsing, The maximum advantage of quantum illumination, Phys. Rev. A **100**, 012327 (2019).

[28] S. Barzanjeh, S. Guha, C. Weedbrook, D. Vitali, J. H. Shapiro, and S. Pirandola, Microwave Quantum Illumination, Phys. Rev. Lett. **114**, 08050 (2015).

[29] S. Barzanjeh, S. Pirandola, D. Vitali, J. M. Fink, Microwave quantum illumination using a digital receiver, Science Advances Vol. 6, no. 19 (2020).

[30] G. De Palma, J. Borregaard, The minimum error probability of quantum illumination, Phys. Rev. A **98**, 012101 (2018).

[31] E. D. Lopaeva, I. Ruo Berchera, I. P. Degiovanni, S. Olivares, G. Brida, M. Genovese, Experimental realisation of quantum illumination, Phys. Rev. Lett. **110**, 153603 (2013)

[32] T. Gregory, P.-A. Moreau, E. Toninelli, and M. J. Padgett, Imaging through noise with quantum illumination, Science Advances, Vol. 6, no. 6, eaay2652 (2020).

[33] M. Sanz, U. Las Heras, J. J. García-Ripoll, E. Solano, and R. Di Candia. Quantum estimation methods for quantum illumination. Phys. Rev. Lett., **118**, 7 (2017).

[34] M. G. A. Paris. Quantum estimation for quantum technology. International Journal of Quantum Information, 07(supp01):125–137 (2009).

[35] In a multiparameter scenario the quantum Fisher information is actually a matrix.

[36] D. Šafránek. Estimation of Gaussian quantum states. Journal of Physics A: Mathematical and Theoretical, 52(3):035304 (2018).

[37] See Supplemental Material.

[38] M. Sanz, K. G. Fedorov, F. Deppe, and E. Solano. Challenges in open-air microwave quantum communication and sensing. 2018 IEEE Conference on Antenna Measurements & Applications (CAMA) (2018).

[39] D. Šafránek, A. R. Lee, and I. Fuentes. Quantum parameter estimation using multi-mode Gaussian states. New Journal of Physics, 17(7):073016 (2015).

[40] C. Eichler, D. Bozyigit, C. Lang, M. Baur, L. Steffen, J. M. Fink, S. Filipp, and A. Wallraff. Observation of two-mode squeezing in the microwave frequency domain. Phys. Rev. Lett., **107** 113601 (2011).

[41] E. Flurin, N. Roch, F. Mallet, M. H. Devoret, and B. Huard. Generating entangled microwave radiation over two transmission lines. Phys. Rev. Lett., **109** 183901 (2012).

[42] S. L. Braunstein and P. van Loock. Quantum information with continuous variables. Rev. Mod. Phys., 77:513–577 (2005).

[43] Note that $N_{\rm S}$ is defined as the expected photon number in a *single* mode, meaning that the actual photon number in the signal is $2N_{\rm S}$.

[44] In a state language this translates to the total unitary being the tensor product of two beam splitters: $U_T(\eta_1,\eta_2) = U(\eta_1)\otimes U(\eta_2)$, with $U(\eta_i)\equiv \exp\left[\arcsin\sqrt{\eta(\omega_i)}(\hat{s}_i^\dagger\hat{b}_i - \hat{s}_i\hat{b}_i^\dagger)\right]$.

[45] G. Adesso, S. Ragy, and A. R. Lee. Continuous variable quantum information: Gaussian states and beyond. Open Systems & Information Dynamics, 21(01n02):1440001 (2014).

[46] U. Las Heras, R. Di Candia, K. G. Fedorov, F. Deppe, M. Sanz, E. Solano. Quantum illumination reveals phase-shift inducing cloaking. Scientific Reports **7**, 9333 (2017).

[47] K. G. Fedorov, S. Pogorzalek, U. Las Heras, M. Sanz, P. Yard, P. Eder, M. Fischer, J. Goetz, E. Xie, K. Inomata, Y. Nakamura, R. Di Candia, E. Solano, A. Marx, F. Deppe, R. Gross. Finite-time quantum entanglement in propagating squeezed microwaves. Sci Rep **8**, 6416 (2018).

[48] R. Dassonneville, R. Assouly, T. Peronnin, P. Rouchon, and B. Huard. Number-resolved photocounter for propagating microwave mode, Phys. Rev. Applied **14**, 044022 (2020).

[49] K. G. Fedorov, L. Zhong, S. Pogorzalek, P. Eder, M. Fischer, J. Goetz, E. Xie, F.Wulschner, K. Inomata, T. Yamamoto, Y. Nakamura, R. Di Candia, U. Las Heras, M. Sanz, E. Solano, E. P. Menzel, F. Deppe, A. Marx, and R. Gross. Displacement of propagating squeezed microwave states. Phys. Rev. Lett., **117** 020502 (2016).

[50] T. González-Raya and M. Sanz Coplanar Antenna Design for Microwave Entangled Signals Propagating in Open Air, arXiv:2009.03021

[51] J. Zhang, T .Li, R. Kokkoniemi, C. Yan, W. Liu, M. Partanen, K. Y. Tan, M. He, L. Ji, L. Grönberg, M. Möttönen, Broadband Tunable Phase Shifter For Microwaves, arXiv:2003.01356.

[52] C. Munuera-Javaloy, I. Arrazola, E. Solano, and J. Casanova Double quantum magnetometry at large static magnetic fields Phys. Rev. B **101**, 104411 (2020).

[53] S. Dambach, B. Kubala, and J. Ankerhold, Generating entangled quantum microwaves in a Josephson-photonics device, New J. Phys. **19**, 023027 (2017).

[54] C. K. Law, I. A. Walmsley, and J. H. Eberly. Continuous frequency entanglement: Effective finite Hilbert space and entropy control. Phys. Rev. Lett., **84** 5304–5307 (2000).

Supplemental Material for Bi-frequency illumination: a quantum-enhanced protocol

QUANTUM FISHER INFORMATION: TWO-MODE SQUEEZED VACUUM STATE

The real covariance matrix of the two-mode squeezed vacuum (TMSV) state, written in the quadrature basis $(\hat{x}_1, \hat{p}_1, \hat{x}_2, \hat{p}_2)$ is

$$\Sigma_{\text{TMSV}} = \begin{bmatrix} \cosh(2r) & 0 & \sinh(2r) & 0 \\ 0 & \cosh(2r) & 0 & -\sinh(2r) \\ \sinh(2r) & 0 & \cosh(2r) & 0 \\ 0 & -\sinh(2r) & 0 & \cosh(2r) \end{bmatrix}, \tag{S1}$$

where $r \in \mathbb{R}_{\geq 0}$ is the *squeezing parameter*. For convenience, we rewrite this in terms of the expected photon number in either of the two modes $N_{\text{S}} = \langle \hat{a}_1^\dagger \hat{a}_1 \rangle = \langle \hat{a}_2^\dagger \hat{a}_2 \rangle$:

$$\begin{bmatrix} 4N_{\text{S}}+1 & 0 & 2\sqrt{2N_{\text{S}}(2N_{\text{S}}+1)} & 0 \\ 0 & 4N_{\text{S}}+1 & 0 & -2\sqrt{2N_{\text{S}}(2N_{\text{S}}+1)} \\ 2\sqrt{2N_{\text{S}}(2N_{\text{S}}+1)} & 0 & 4N_{\text{S}}+1 & 0 \\ 0 & -2\sqrt{2N_{\text{S}}(2N_{\text{S}}+1)} & 0 & 4N_{\text{S}}+1 \end{bmatrix}. \tag{S2}$$

Assuming an equal expected thermal photon number for the two noisy environments, the corresponding covariance matrix is $\Sigma_{\text{th}} \oplus \Sigma_{\text{th}}$, where

$$\Sigma_{\text{th}} = \begin{bmatrix} 2N_{\text{th}}+1 & 0 \\ 0 & 2N_{\text{th}}+1 \end{bmatrix} \tag{S3}$$

is the covariance matrix of one thermal mode. The assumption of equal thermal photon number is accurate as long as the frequency difference $\omega_2 - \omega_1$ is sufficiently small. To make this statement more quantitative, let us assume two different thermal photon densities, N_1 and N_2. The Bose-Einstein distribution for photons is $N_i \propto 1/e^{\beta\omega_i - 1}$ where $\beta \equiv \hbar/k_B T$ is a function of the temperature T. Then,

$$\frac{N_1}{N_2} = \frac{e^{\beta\omega_1 - 1}}{e^{\beta\omega_2 - 1}} = \frac{1}{1 + \frac{\beta\Delta\omega e^{\beta\omega_1}}{e^{\beta\omega_1}-1}}, \tag{S4}$$

where $\Delta\omega \equiv \omega_2 - \omega_1$. Up to first order in $\beta\Delta\omega$, the last expression reduces to $1 - \Delta\omega/\omega_1$. This means that $N_1 \approx N_2$ if $\Delta\omega/\omega_1 \ll 1$. In particular, for $T = 300$ K and $\omega_1/2\pi = 5$ GHz the expected thermal photon number is roughly 1250. It is straightforward to check that for these frequencies and temperatures, the above approximations are good (*i.e.* $\sim 4\%$ of relative error) for frequency differences up to 20%.

To construct the whole initial (real) covariance matrix we will rearrange the Hilbert subspaces by frequencies, in the following way: "bath + signal + bath + signal". This is convenient because the interaction is by assumption frequency non-mixing. The total covariance matrix of the input mode is then

$$\begin{bmatrix} \Sigma_{\text{th}} & 0 & 0 & 0 \\ 0 & (4N_{\text{S}}+1)\mathbb{1}_2 & 0 & 2\sqrt{2N_{\text{S}}(2N_{\text{S}}+1)}\sigma_Z \\ 0 & 0 & \Sigma_{\text{th}} & 0 \\ 0 & 2\sqrt{2N_{\text{S}}(2N_{\text{S}}+1)}\sigma_Z & 0 & (4N_{\text{S}}+1)\mathbb{1}_2 \end{bmatrix}, \tag{S5}$$

where σ_Z is the Pauli Z matrix and $\mathbb{1}_n$ is the $n \times n$ identity matrix.

If the interaction with the object is frequency non-mixing, each mode in the bi-frequency state sees a beam splitter with reflectivity $\eta(\omega_i)$ with $i = 1, 2$ defining the two frequencies. In the symplectic formalism, the total interaction is thus obtained by the direct sum of each beam-splitter transformation: $S_{\text{T}} = S_{\text{BS}}(\eta_1) \oplus S_{\text{BS}}(\eta_2)$, where

$$S_{\text{BS}}(\eta_i) := \begin{bmatrix} \sqrt{\eta_i}\mathbb{1}_2 & \sqrt{1-\eta_i}\mathbb{1}_2 \\ -\sqrt{1-\eta_i}\mathbb{1}_2 & \sqrt{\eta_i}\mathbb{1}_2 \end{bmatrix}. \tag{S6}$$

The full, transformed state is finally characterised by the covariance matrix

$$S_{\mathrm{T}}\Sigma_{\mathrm{TMSV}}S_{\mathrm{T}}^{\intercal}=\begin{bmatrix} A(\eta_1)\mathbb{1}_2 & B(\eta_1)\mathbb{1}_2 & f(1-\eta_1,1-\eta_2)\sigma_Z & f(1-\eta_1,\eta_2)\sigma_Z \\ B(\eta_1)\mathbb{1}_2 & C(\eta_1)\mathbb{1}_2 & f(\eta_1,1-\eta_2)\sigma_Z & f(\eta_1,\eta_2)\sigma_Z \\ f(1-\eta_1,1-\eta_2)\sigma_Z & f(\eta_1,1-\eta_2)\sigma_Z & A(\eta_2)\mathbb{1}_2 & B(\eta_2)\mathbb{1}_2 \\ f(1-\eta_1,\eta_2)\sigma_Z & f(\eta_1,\eta_2)\sigma_Z & B(\eta_2)\mathbb{1}_2 & C(\eta_2)\mathbb{1}_2 \end{bmatrix}, \tag{S7}$$

where

$$\begin{aligned} f(x,y) &= 2\sqrt{2N_{\mathrm{S}}(2N_{\mathrm{S}}+1)xy} \\ A(x) &= 2x(N_{\mathrm{th}}-2N_{\mathrm{S}})+4N_{\mathrm{S}}+1 \\ B(x) &= 2\sqrt{(1-x)\,x}(2N_{\mathrm{S}}-N_{\mathrm{th}}) \\ C(x) &= 2x(2N_{\mathrm{S}}-N_{\mathrm{th}})+2N_{\mathrm{th}}+1 \end{aligned}$$

and σ_Z is the fourth Pauli matrix. The received state is obtained by partial tracing the losses, which in our construction correspond to the first and third modes. In the symplectic formalism, partial traces are performed by removing the corresponding rows and columns [S1]. We are thus left with the following state:

$$\begin{bmatrix} C(\eta_1)\mathbb{1}_2 & f(\eta_1,\eta_2)\sigma_Z \\ f(\eta_1,\eta_2)\sigma_Z & C(\eta_2)\mathbb{1}_2 \end{bmatrix}. \tag{S8}$$

The reparametrization of the state in terms of $\lambda=\eta_2-\eta_1$ is simply

$$\Sigma_\lambda=\begin{bmatrix} C(\eta_1)\mathbb{1}_2 & f(\eta_1,\eta_1+\lambda)\sigma_Z \\ f(\eta_1,\eta_1+\lambda)\sigma_Z & C(\eta_1+\lambda)\mathbb{1}_2 \end{bmatrix}. \tag{S9}$$

Note that, in the absence of beam splitter, i.e., when $\eta_1=0=\lambda$ we have that the received state is a pair of thermal modes, each with its corresponding frequency: $C(0)=1+2N_{\mathrm{th}}$ and $f(0,0)=0$. This is what should be expected, since the received state is precisely the *reflected* part of the signal. To compute the quantum Fisher information we follow [S2]:

$$\begin{aligned} H(\lambda)=\frac{1}{2(\det[A]-1)}&\left[\det[A]\,\mathrm{Tr}\left[(A^{-1}\partial_\lambda A)^2\right]+\sqrt{\det[\mathbb{1}_2+A^2]}\,\mathrm{Tr}\left[\left((\mathbb{1}_2+A^2)^{-1}\right)^2\right]\right. \\ &\left.-\,4\left(\nu_+^2-\nu_-^2\right)\left(\frac{(\partial_\lambda\nu_+)^2}{\nu_+^4-1}-\frac{(\partial_\lambda\nu_-)^2}{\nu_-^4-1}\right)+2\partial_\lambda\vec{d}^{\,\dagger}\Sigma_\lambda^{-1}\partial_\lambda\vec{d}\right], \end{aligned} \tag{S10}$$

where the *symplectic eigenvalues* of Σ_λ are defined by

$$\nu_\pm:=\frac{1}{2}\sqrt{\mathrm{Tr}[A^2]\pm\sqrt{\left(\mathrm{Tr}[A^2]\right)^2-16\det[A]}}, \tag{S11}$$

where the matrix A is given by $A:=i\Omega T\Sigma_\lambda T^\intercal$ and $T_{ij}:=\delta_{j+4,2i}+\delta_{j,2i-1}$ is the matrix that changes the basis to the *quadrature basis* $(\hat{x}_1^{\mathrm{th}},\hat{x}_1^{\mathrm{S}},\hat{x}_2^{\mathrm{th}},\hat{x}_2^{\mathrm{S}},\hat{p}_1^{\mathrm{th}},\hat{p}_1^{\mathrm{S}},\hat{p}_2^{\mathrm{th}},\hat{p}_2^{\mathrm{S}})^\intercal$, and

$$\mathbf{\Omega}:=\begin{bmatrix} 0 & \mathbb{1}_2 \\ -\mathbb{1}_2 & 0 \end{bmatrix}.$$

We have that

$$A=i\begin{bmatrix} 0 & 0 & C(\eta_1) & -f(\eta_1,\eta_1+\lambda) \\ 0 & 0 & -f(\eta_1,\eta_1+\lambda) & C(\eta_1+\lambda) \\ -C(\eta_1) & -f(\eta_1,\eta_1+\lambda) & 0 & 0 \\ -f(\eta_1,\eta_1+\lambda) & -C(\eta_1+\lambda) & 0 & 0 \end{bmatrix}, \tag{S12}$$

and the symplectic eigenvalues

$$\begin{aligned}\frac{\nu_\pm^2}{2\lambda(N_{\text{th}}-2N_{\text{S}})} =& \sqrt{4\lambda^2N_{\text{S}}^2+4N_{\text{S}}(\lambda-2\eta_1(\eta_1+\lambda-1))-2N_{\text{th}}(2\eta_1+\lambda-2)(2N_{\text{S}}(2\eta_1+\lambda)+1)+N_{\text{th}}^2(2\eta_1+\lambda-2)^2+1}\\ &-8\eta_1^2N_{\text{S}}+8\eta_1N_{\text{S}}-2\lambda\left(2(2\eta_1-1)N_{\text{S}}(2N_{\text{th}}+1)-2(\eta_1-1)N_{\text{th}}^2+N_{\text{th}}\right)\\ &-4(\eta_1-1)N_{\text{th}}(4\eta_1N_{\text{S}}+1)+2\lambda^2(N_{\text{th}}-2N_{\text{S}})^2+4(\eta_1-1)^2N_{\text{th}}^2+1.\end{aligned} \tag{S13}$$

The symplectic eigenvalues are both larger than one for every N_{th}, N_{S} and η_1, so there is no need to use any regularization procedure. Indeed, this is due to the mixedness of the received state: regularization is only needed for pure states. The two-sided limit of the QFI when the parameter λ goes to zero is

$$\begin{aligned}H_Q = k^{-1}&\left[8\tau_1\eta_1N_{\text{S}}^3(2N_{\text{th}}+1)+4N_{\text{S}}^2\left(-\eta_1+(\eta_1+3\eta_1N_{\text{th}})^2-\eta_1N_{\text{th}}(10N_{\text{th}}+7)+3N_{\text{th}}(N_{\text{th}}+1)+1\right)\right.\\ &-2N_{\text{S}}N_{\text{th}}(-\eta_1+N_{\text{th}}(\eta_1(3\eta_1-8)+4\tau_1(\tau_1-\eta_1)N_{\text{th}}+3)+1)\\ &\left.+N_{\text{th}}^2(2\tau_1N_{\text{th}}(\tau_1N_{\text{th}}+1)+1)\right],\end{aligned} \tag{S14}$$

where

$$k=\tau_1(N_{\text{th}}(4N_{\text{S}}\eta_1+N_{\text{th}}\tau_1+1)+2N_{\text{S}}\eta_1)\left(2N_{\text{th}}\tau_1(4N_{\text{S}}\eta_1+1)+4N_{\text{S}}\eta_1\tau_1+2N_{\text{th}}^2\tau_1^2+1\right), \tag{S15}$$

and $\tau_1 := 1-\eta_1$.

QUANTUM FISHER INFORMATION: COHERENT STATES

We reproduce the same calculations for the coherent pair now. Noting that every coherent state, following our conventions, has a covariance matrix given by the identity, the real covariance matrix in the quadrature basis is

$$\begin{bmatrix}\Sigma_{\text{th}} & 0 & 0 & 0\\ 0 & \mathbb{1}_2 & 0 & 0\\ 0 & 0 & \Sigma_{\text{th}} & 0\\ 0 & 0 & 0 & \mathbb{1}_2\end{bmatrix}, \tag{S16}$$

while the displacement vector is $\vec{d}^{\mathsf{T}} = \left[0,0,\sqrt{2}\alpha,0,0,0,\sqrt{2}\alpha,0\right]$, where $|\alpha|^2 = N_{\text{S}}$. The transformed displacement vector is then

$$S_T\vec{d} = \left[\alpha\sqrt{2\tau_1},0,\alpha\sqrt{2\eta_1},0,\alpha\sqrt{2}\sqrt{\tau_1-\lambda},0,\alpha\sqrt{2}\sqrt{\eta_1+\lambda},0\right]^{\mathsf{T}} \tag{S17}$$

The transformed, and already reduced covariance matrix is (*i.e.* after partial tracing the losses)

$$\begin{bmatrix}(1+2\tau_1N_{\text{th}})\mathbb{1}_2 & 0\\ 0 & 1-2N_{\text{th}}(\lambda-\tau_1)\mathbb{1}_2\end{bmatrix} \tag{S18}$$

The matrix A is

$$A = i\begin{bmatrix}0 & 0 & 1+2N_{\text{th}}\tau_1 & 0\\ 0 & 0 & 0 & 1-2N_{\text{th}}(\lambda-\tau_1)\\ -1-2N_{\text{th}}\tau_1 & 0 & 0 & 0\\ 0 & -1+2N_{\text{th}}(\lambda-\tau_1) & 0 & 0\end{bmatrix} \tag{S19}$$

The symplectic eigenvalues are

$$\nu_\pm = \sqrt{\pm2\sqrt{\lambda^2N_{\text{th}}^2(N_{\text{th}}(\lambda+\eta_1-\tau_1)-1)^2}+2N_{\text{th}}\left(-\lambda+N_{\text{th}}\left(\lambda^2-2\lambda\tau_1\right)+2\tau_1^2\right)-2\eta_1+2)+1}. \tag{S20}$$

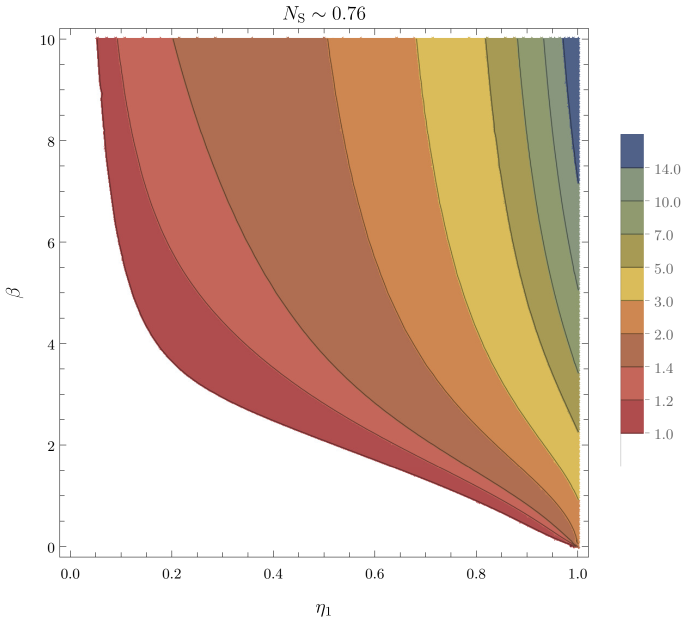

FIG. S1. Quantum Fisher information ratio H_Q/H_C as a function of the noise factor $\beta := N_S/N_{th}$ and the reflectivity η_1 for an experimentally reasonable two-mode squeezing of $N_S \sim 0.76$. As in previous diagrams, white represents no gain. The protocol becomes more noise-resilient in the highly reflective region, *i.e.* for smaller β.

Again, the symplectic eigenvalues are always larger than one in the coherent case, so no regularization of the QFI is needed. The QFI in the limit when $\lambda \to 0$ is

$$H_C = \frac{\alpha^2}{\eta_1(1+2N_{th}\tau_1)} + \frac{N_{th}}{\tau_1(\tau_1 N_{th}+1)}. \tag{S21}$$

In the following we take $\alpha = \sqrt{N_S}$. The ratio of the two QFIs converges to the following

$$\lim_{\substack{\lambda\to 0\\ \eta_1\to 1}} H_Q/H_C = \frac{N_S^2(8N_{th}(N_{th}+1)+4)+4N_S N_{th}^2 + N_{th}^2}{N_{th}(N_S(4N_{th}+2)+N_{th})} \tag{S22}$$

In particular, in the noise-dominated regime $N_{th} \gg 1$ the above expression converges to

$$1 + \frac{8N_S^2}{1+4N_S}. \tag{S23}$$

When $N_S = 0$ the ratio converges to one, meaning there is no advantage in entanglement if there is nothing to entangle. The protocol is then safe from any shadow-effect.

OPTIMAL OBSERVABLE: TWO-MODE SQUEEZED VACUUM STATE

In the main text we obtained an expression for the optimal quantum observable, $\hat{O}_Q = L_{11}\hat{a}_1^\dagger\hat{a}_1 + L_{22}\hat{a}_2^\dagger\hat{a}_2 + L_{12}\left(\hat{a}_1^\dagger\hat{a}_2^\dagger + \hat{a}_1\hat{a}_2\right) + L_0\mathbb{1}_{12}$, and gave only the coefficient values in the high reflectivity and noiseless case. Here we give the general expressions:

$$
\begin{aligned}
L11 &= -\frac{2\eta_1 N_{\mathrm{S}} \left(2N_{\mathrm{S}}+1\right) \left(2N_{\mathrm{th}}+1\right)}{-A+B-C+D} \\
L22 &= \frac{4\eta_1 \left(2\eta_1-1\right) N_{\mathrm{S}}^2 \left(2N_{\mathrm{th}}+1\right) + 2N_{\mathrm{S}} \left(\eta_1 - 2N_{\mathrm{th}} \left(\left(\eta_1-3\right)\eta_1 + \left(\eta_1-1\right)\left(3\eta_1-1\right)N_{\mathrm{th}}+1\right)-1\right) + N_{\mathrm{th}} \left(2\left(\eta_1-1\right)N_{\mathrm{th}}\left(\left(\eta_1-1\right)N_{\mathrm{th}}-1\right)+1\right)}{A-B+C-D} \\
L12 &= -\frac{\sqrt{2}\sqrt{N_{\mathrm{S}}\left(2N_{\mathrm{S}}+1\right)}\left(\eta_1^2\left(N_{\mathrm{S}}\left(4N_{\mathrm{th}}+2\right)-N_{\mathrm{th}}^2\right)+N_{\mathrm{th}}\left(N_{\mathrm{th}}+1\right)\right)}{A-B+C-D} \\
L_0 &= -\frac{4\eta_1^3\left(N_{\mathrm{th}}^2-2N_{\mathrm{S}}\left(2N_{\mathrm{th}}+1\right)\right)^2 - 2\eta_1^2\left(6N_{\mathrm{th}}+5\right)F\left(N_{\mathrm{S}}\left(4N_{\mathrm{th}}+2\right)-N_{\mathrm{th}}^2\right) + 4\eta_1\left(N_{\mathrm{th}}+1\right)\left(N_{\mathrm{S}}^2\left(8N_{\mathrm{th}}+4\right)-2N_{\mathrm{S}}\left(N_{\mathrm{th}}\left(6N_{\mathrm{th}}+5\right)+1\right)+N_{\mathrm{th}}^2\left(3N_{\mathrm{th}}+2\right)\right)+\left(2N_{\mathrm{th}}+3\right)GF}{E-4\eta_1\left(2N_{\mathrm{th}}+1\right)F\left(-4N_{\mathrm{S}}N_{\mathrm{th}}+N_{\mathrm{S}}\left(2N_{\mathrm{S}}-1\right)+N_{\mathrm{th}}^2\right)-8N_{\mathrm{S}}^2\left(3N_{\mathrm{th}}\left(N_{\mathrm{th}}+1\right)+1\right)+4N_{\mathrm{S}}N_{\mathrm{th}}\left(N_{\mathrm{th}}\left(4N_{\mathrm{th}}+3\right)+1\right)-2N_{\mathrm{th}}^2 G},
\end{aligned}
$$

where

$$
\begin{aligned}
A &\equiv 8\left(\eta_1-1\right)\eta_1 N_{\mathrm{S}}^3\left(2N_{\mathrm{th}}+1\right) \\
B &\equiv 4N_{\mathrm{S}}^2\left(-\eta_1+\left(\eta_1+3\eta_1 N_{\mathrm{th}}\right)^2-\eta_1 N_{\mathrm{th}}\left(10N_{\mathrm{th}}+7\right)+3N_{\mathrm{th}}\left(N_{\mathrm{th}}+1\right)+1\right) \\
C &\equiv 2N_{\mathrm{S}}N_{\mathrm{th}}\left(-\eta_1+N_{\mathrm{th}}\left(\eta_1\left(3\eta_1-8\right)+4\left(\eta_1-1\right)\left(2\eta_1-1\right)N_{\mathrm{th}}+3\right)+1\right) \\
D &\equiv N_{\mathrm{th}}^2\left(2\left(\eta_1-1\right)N_{\mathrm{th}}\left(\left(\eta_1-1\right)N_{\mathrm{th}}-1\right)+1\right) \\
E &\equiv 4\eta_1^2\left(-4N_{\mathrm{S}}N_{\mathrm{th}}+N_{\mathrm{S}}\left(2N_{\mathrm{S}}-1\right)+N_{\mathrm{th}}^2\right)\left(N_{\mathrm{S}}\left(4N_{\mathrm{th}}+2\right)-N_{\mathrm{th}}^2\right) \\
F &\equiv 2N_{\mathrm{S}}-N_{\mathrm{th}} \\
G &\equiv 2N_{\mathrm{th}}\left(N_{\mathrm{th}}+1\right)+1
\end{aligned}
$$

In the high reflectivity case $\eta_1 \to 1$ we find:

$$
\begin{aligned}
\lim_{\eta_1\to 1} L_{11} &= -\frac{2N_{\mathrm{S}}(2N_{\mathrm{S}}+1)(2N_{\mathrm{th}}+1)}{N_{\mathrm{S}}^2(8N_{\mathrm{th}}(N_{\mathrm{th}}+1)+4)+4N_{\mathrm{S}}N_{\mathrm{th}}^2+N_{\mathrm{th}}^2} \\
\lim_{\eta_1\to 1} L_{22} &= -\frac{4N_{\mathrm{S}}(2N_{\mathrm{S}}N_{\mathrm{th}}+N_{\mathrm{S}}+N_{\mathrm{th}})+N_{\mathrm{th}}}{N_{\mathrm{S}}^2(8N_{\mathrm{th}}(N_{\mathrm{th}}+1)+4)+4N_{\mathrm{S}}N_{\mathrm{th}}^2+N_{\mathrm{th}}^2} \\
\lim_{\eta_1\to 1} L_{12} &= \frac{2\sqrt{2}\sqrt{N_{\mathrm{S}}(2N_{\mathrm{S}}+1)}(N_{\mathrm{S}}(4N_{\mathrm{th}}+2)+N_{\mathrm{th}})}{N_{\mathrm{S}}^2(8N_{\mathrm{th}}(N_{\mathrm{th}}+1)+4)+4N_{\mathrm{S}}N_{\mathrm{th}}^2+N_{\mathrm{th}}^2} \\
\lim_{\eta_1\to 1} L_0 &= \frac{-2N_{\mathrm{S}}(N_{\mathrm{S}}(8N_{\mathrm{th}}+4)+6N_{\mathrm{th}}+1)-3N_{\mathrm{th}}}{8N_{\mathrm{S}}^2(2N_{\mathrm{th}}(N_{\mathrm{th}}+1)+1)+8N_{\mathrm{S}}N_{\mathrm{th}}^2+2N_{\mathrm{th}}^2}
\end{aligned}
$$

Additionally, as shown in the main text, in the noiseless case we get

$$
\begin{aligned}
\lim_{\substack{N_{\mathrm{th}}\to 0 \\ \eta_1\to 1}} \hat{O}_Q &= -\mu^2 \hat{a}_1^\dagger \hat{a}_1 - \hat{a}_2^\dagger \hat{a}_2 + \mu\left(\hat{a}_1^\dagger \hat{a}_2^\dagger + \hat{a}_1 \hat{a}_2\right) - \nu \mathbb{1}_{12} \\
&\equiv \hat{b}_1^\dagger \hat{b}_1 - 1,
\end{aligned}
$$

where $\mu^2 \equiv (1+1/2N_{\mathrm{S}})$ and $\nu \equiv (1+1/4N_{\mathrm{S}})$ and

$$
\hat{b}_1 \equiv -i\left(\hat{a}_2^\dagger - \mu \hat{a}_1\right). \tag{S24}
$$

An scheme of the implementation of this observable can be seen in FIG. S2. After the first beam splitter we have

$$
\begin{aligned}
\hat{a}_1' &= \cos\varphi \hat{a}_1 + \sin\varphi \hat{a}_2 \\
\hat{a}_2' &= -\sin\varphi \hat{a}_1 + \cos\varphi \hat{a}_2,
\end{aligned} \tag{S25}
$$

then the Josephson parametric amplifiers (JPA) ideally are squeezing operators, acting as

$$
\hat{a}_i'' = S(r_i,\theta_i)^\dagger \hat{a}_i' S(r_i,\theta_i) \tag{S26}
$$

where $S(r_i,\theta_i)$ is the squeezing operator, acting as

$$
\begin{aligned}
S(r_i,\theta_i)^\dagger \hat{a}_i' S(r_i,\theta_i) &= \cosh r_i \hat{a}_i' - e^{i\theta_i}\sinh r_i \hat{a}_i^\dagger \\
S(r_i,\theta_i)^\dagger \hat{a}_i'^\dagger S(r_i,\theta_i) &= \cosh r_i \hat{a}_i'^\dagger - e^{-i\theta_i}\sinh r_i \hat{a}_i.
\end{aligned}
$$

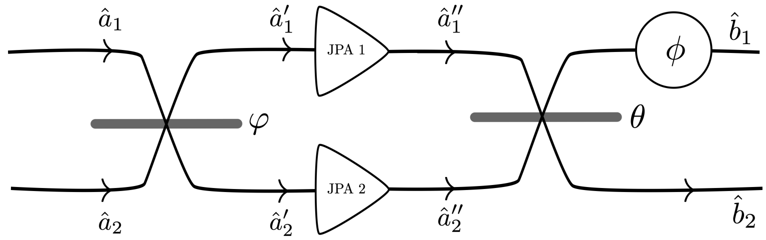

FIG. S2. Schematic circuit for the generation of mode $\hat{b}_1$, needed to correctly implement the optimal observable in the two-mode squeezed vacuum (TMSV) state. The original $\hat{a}_i$ modes mix at a φ beam splitter, and the outputs go through a single-mode squeezing operator – Josephson parametric amplifier (JPA) in microwaves, with parameters r_i and θ_i corresponding to squeezing and phase. Then they mix at a second beam splitter θ. A phase shift ϕ is applied at the end, to cancel undesired terms.

Assuming that the phase shifter ϕ acts as $\hat{c} \mapsto e^{-i\phi}\hat{c}$ we find the following output modes

$$\begin{aligned} e^{i\phi}\hat{b}_1 &= \cos\theta\left(\cosh r_1 \hat{a}_1' - e^{i\theta_1}\sinh r_1 \hat{a}_1^\dagger\right) + \sin\theta\left(\cosh r_2 \hat{a}_2' - e^{i\theta_2}\sinh r_2 \hat{a}_2^\dagger\right) \\ \hat{b}_2 &= -\sin\theta\left(\cosh r_1 \hat{a}_1' - e^{i\theta_1}\sinh r_1 \hat{a}_1^\dagger\right) + \cos\theta\left(\cosh r_2 \hat{a}_2' - e^{i\theta_2}\sinh r_2 \hat{a}_2^\dagger\right). \end{aligned}$$

We insert (S25) in the last expression and regroup, finding

$$\begin{aligned} e^{i\phi}\hat{b}_1 &= \cos\theta\left(\cosh r_1(\cos\varphi\hat{a}_1 + \sin\varphi\hat{a}_2) - e^{i\theta_1}\sinh r_1 \hat{a}_1^\dagger\right) \\ &\quad + \sin\theta\left(\cosh r_2(-\sin\varphi\hat{a}_1 + \cos\varphi\hat{a}_2) - e^{i\theta_2}\sinh r_2 \hat{a}_2^\dagger\right) \\ &= \hat{a}_1\left(\cos\theta\cos\varphi\cosh r_1 - \sin\theta\sin\varphi\cosh r_2\right) \\ &\quad + \hat{a}_2\left(\cos\theta\sin\varphi\cosh r_1 + \sin\theta\cos\varphi\cosh r_2\right) \\ &\quad + \hat{a}_1^\dagger\left(-e^{i\theta_1}\cos\theta\cos\varphi\sinh r_1 + e^{i\theta_2}\sin\theta\sin\varphi\sinh r_2\right) \\ &\quad + \hat{a}_2^\dagger\left(-e^{i\theta_1}\cos\theta\sin\varphi\sinh r_1 - e^{i\theta_2}\sin\theta\cos\varphi\sinh r_2\right) \end{aligned}$$

Because we want to perform photon-counting over the operator in Eq. (S24), we identify:

$$i\mu = \cos\theta\cos\varphi\cosh r_1 - \sin\theta\sin\varphi\cosh r_2 \tag{S27}$$

$$i = e^{i\theta_1}\cos\theta\sin\varphi\sinh r_1 + e^{i\theta_2}\sin\theta\cos\varphi\sinh r_2. \tag{S28}$$

OPTIMAL OBSERVABLE: COHERENT STATES

The optimal observable in this case is given by

$$\hat{O}_C = A\mathbb{1}_{(1)} \otimes \left(2\hat{a}_2^\dagger\hat{a}_2 - 2\eta_1\sqrt{\alpha}(\hat{a}_2 + \hat{a}_2^\dagger) + 1 + 2\eta_1^2\alpha\right), \tag{S29}$$

where $A = 1/2(\eta_1 - 1)(1 - N_{\text{th}}(\eta_1 - 1))$ and $\mathbb{1}_{(1)}$ is the absence of active measurement of mode 1. This expression can be rearranged as $\hat{O}_C = 2A\mathbb{1}_{(1)} \otimes \left[\left(\hat{a}_2^\dagger - \eta_1\sqrt{\alpha}\right)\left(\hat{a}_2 - \eta_1\sqrt{\alpha}\right) + \frac{1}{2}\right]$. This operator can be experimentally performed with a displacement $D(-\eta_1\sqrt{\alpha})$ and photon-counting in the resulting mode.

Test of the methods: Quantum Illumination As a test of the methods, we reproduce known results from quantum illumination [S3], providing some new insight. In quantum illumination, an entangled bipartite state is generated in the lab, and one of the parts (the signal) is sent towards a noisy region where there may be a slightly reflective target. The other part (the idler) is kept for future reference. The (possibly) reflected signal, mixed with the environmental thermal noise is collected back, and a joint measurement of this reflected signal together with the idler is performed. It has been shown, both theoretically and experimentally, that this approach achieves sensitivities which are impossible to get in the classical world, *i.e.* when one does not use entanglement. One way to show this quantum enhancement is by computing the quantum Fisher information for both cases, and analyzing their ratio, provided that the same amount of energy is sent towards the target. If, for example, one uses a two-mode squeezed vacuum state for quantum illumination, the number of photons in the classical state should be equal to half of the total photon number in the TMSV state. An important remark is that one has to compare with the best classical protocol. It has been shown that this corresponds to illumination with coherent states.

We shall proceed to prove these results with our approach. The initial (real) covariance matrix is

$$\Sigma_{\text{TMSV}} = \begin{bmatrix} 2N_{\text{th}}+1 & 0 & 0 & 0 & 0 & 0 \\ 0 & 2N_{\text{th}}+1 & 0 & 0 & 0 & 0 \\ 0 & 0 & 2N_{\text{S}}+1 & 0 & 2\sqrt{N_{\text{S}}(N_{\text{S}}+1)} & 0 \\ 0 & 0 & 0 & 2N_{\text{S}}+1 & 0 & -2\sqrt{N_{\text{S}}(N_{\text{S}}+1)} \\ 0 & 0 & 2\sqrt{N_{\text{S}}(N_{\text{S}}+1)} & 0 & 2N_{\text{S}}+1 & 0 \\ 0 & 0 & 0 & -2\sqrt{N_{\text{S}}(N_{\text{S}}+1)} & 0 & 2N_{\text{S}}+1 \end{bmatrix}, \tag{S30}$$

where we have ordered the modes as: thermal state, signal, and idler. Here N_{S} is the *signal* photon number: $N_{\text{S}} := \langle \hat{a}_{\text{S}}^\dagger \hat{a}_{\text{S}} \rangle$.

The symplectic transformation of quantum illumination is $S = S_{\text{BS}}^{(\text{B, S})}(\eta) \oplus \mathbb{1}^{(\text{I})}$, *i.e.*, a beam splitter of reflectivity η mixing bath and signal, and no interaction for the idler mode. In matrix form, this transformation reads

$$S(\eta) = \begin{bmatrix} \sqrt{\eta} & 0 & \sqrt{1-\eta} & 0 & 0 & 0 \\ 0 & \sqrt{\eta} & 0 & \sqrt{1-\eta} & 0 & 0 \\ -\sqrt{1-\eta} & 0 & \sqrt{\eta} & 0 & 0 & 0 \\ 0 & -\sqrt{1-\eta} & 0 & \sqrt{\eta} & 0 & 0 \\ 0 & 0 & 0 & 0 & 1 & 0 \\ 0 & 0 & 0 & 0 & 0 & 1 \end{bmatrix}, \tag{S31}$$

meaning that the first two modes (thermal and signal) get mixed at a beam splitter, and the idler remains intact. The total, transformed state is

$$\begin{bmatrix} (-2(\eta-1)N_{\text{S}}+2\eta N_{\text{th}}+1)\,\mathbb{1} & 2\sqrt{(1-\eta)\eta}(N_{\text{S}}-N_{\text{th}})\mathbb{1} & 2\sqrt{1-\eta}\sqrt{N_{\text{S}}(N_{\text{S}}+1)}\sigma_Z \\ 2\sqrt{(1-\eta)\eta}(N_{\text{S}}-N_{\text{th}})\mathbb{1} & (2\eta N_{\text{S}}-2(\eta-1)N_{\text{th}}+1)\,\mathbb{1} & 2\sqrt{\eta}\sqrt{N_{\text{S}}(N_{\text{S}}+1)}\sigma_Z \\ 2\sqrt{1-\eta}\sqrt{N_{\text{S}}(N_{\text{S}}+1)}\sigma_Z & 2\sqrt{\eta}\sqrt{N_{\text{S}}(N_{\text{S}}+1)}\sigma_Z & (2N_{\text{S}}+1)\,\mathbb{1} \end{bmatrix} \tag{S32}$$

After tracing out the losses, we receive the state:

$$\Sigma_\eta = \begin{bmatrix} 2\eta N_{\text{S}}-2(\eta-1)N_{\text{th}}+1 & 0 & 2\sqrt{\eta}\sqrt{N_{\text{S}}(N_{\text{S}}+1)} & 0 \\ 0 & 2\eta N_{\text{S}}-2(\eta-1)N_{\text{th}}+1 & 0 & -2\sqrt{\eta}\sqrt{N_{\text{S}}(N_{\text{S}}+1)} \\ 2\sqrt{\eta}\sqrt{N_{\text{S}}(N_{\text{S}}+1)} & 0 & 2N_{\text{S}}+1 & 0 \\ 0 & -2\sqrt{\eta}\sqrt{N_{\text{S}}(N_{\text{S}}+1)} & 0 & 2N_{\text{S}}+1 \end{bmatrix} \tag{S33}$$

We can check this is correct since for $\eta = 0$ we simply get two thermal states with zero quantum correlations.

In order to agree with the original formulation of the problem, we will substitute $\eta \to \eta^2$ in what follows. Therefore, the matrix A , defined as $A := i\Omega T \Sigma_{\eta^2} T^{\intercal}$, where and $\Omega := \text{antidiag}(\mathbb{1}_2, -\mathbb{1}_2)$, and $T_{ij} := \delta_{j+4,2i} + \delta_{j,2i-1}$ is the matrix that changes the basis to the *quadrature basis*, results in

$$A = i \begin{bmatrix} 0 & 0 & 2\eta^2(N_{\text{S}}-N_{\text{th}})+2N_{\text{th}}+1 & -2\eta\sqrt{N_{\text{S}}(N_{\text{S}}+1)} \\ 0 & 0 & -2\eta\sqrt{N_{\text{S}}(N_{\text{S}}+1)} & 2N_{\text{S}}+1 \\ 2\eta^2(N_{\text{th}}-N_{\text{S}})-2N_{\text{th}}-1 & -2\eta\sqrt{N_{\text{S}}(N_{\text{S}}+1)} & 0 & 0 \\ -2\eta\sqrt{N_{\text{S}}(N_{\text{S}}+1)} & -2N_{\text{S}}-1 & 0 & 0 \end{bmatrix} \tag{S34}$$

$$\begin{aligned} \frac{\nu_\pm^2}{2\left(\eta^2-1\right)|N_{\text{S}}-N_{\text{th}}|} =& \sqrt{-2\eta^2\left(N_{\text{S}}^2+N_{\text{S}}+N_{\text{th}}^2+N_{\text{th}}\right)+\eta^4(N_{\text{S}}-N_{\text{th}})^2+(N_{\text{S}}+N_{\text{th}}+1)^2} \\ & -2\eta^2\left(2N_{\text{S}}^2-2N_{\text{S}}N_{\text{th}}+N_{\text{S}}+2N_{\text{th}}^2+N_{\text{th}}\right) \\ & +2\eta^4(N_{\text{S}}-N_{\text{th}})^2+2N_{\text{S}}(N_{\text{S}}+1)+2N_{\text{th}}(N_{\text{th}}+1)+1 \end{aligned} \tag{S35}$$

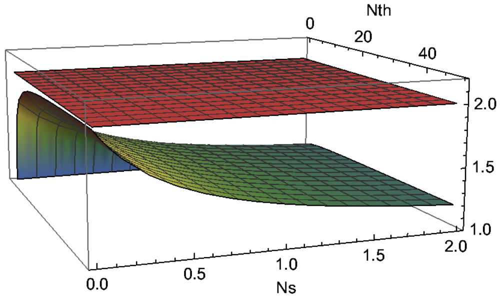

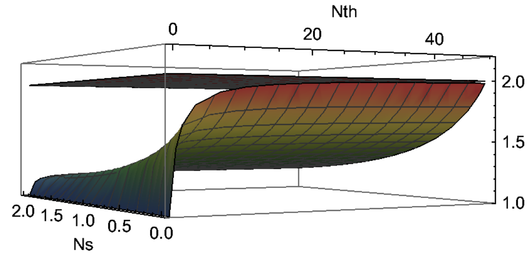

FIG. S3. Two views of the same quantum Fisher information ratio H_Q/H_C for the problem of quantum illumination in the case of a low reflective object. The red plane represents $H_Q = 2H_C$, which is asymptotically achieved in the highly noisy, and dim signal scenario, *i.e.* when $N_{\text{th}} \to \infty$ and $N_{\text{S}} \to 0$.

Using this in equation (S10) and taking the limit $\eta \to 0$ we find

$$\lim_{\eta\to 0} H_Q(\eta) \equiv H_Q = \frac{4N_{\text{S}}(N_{\text{S}}+1)}{2N_{\text{S}}N_{\text{th}} + N_{\text{S}} + N_{\text{th}} + 1} \tag{S36}$$

confirming previously obtained analytical results. In the coherent probe case, using equation (S10) we find

$$H_C(\eta) = \frac{4N_{\text{S}}}{1-2N_{\text{th}}(\eta-1)} + \frac{4N_{\text{th}}\eta^2}{(\eta^2-1)\left(N_{\text{th}}\left(\eta^2-1\right)-1\right)}, \tag{S37}$$

taking the limit of low reflectivity $\eta \to 1$ we find $H_C(\eta = 0) \equiv H_C = 4Ns/(1+2Nth)$. Computing the ratio of Eqs. (S36) and (S37) we obtain:

$$\frac{H_Q}{H_C} = \frac{(N_{\text{S}}+1)(2N_{\text{th}}+1)}{2N_{\text{S}}N_{\text{th}} + N_{\text{S}} + N_{\text{th}} + 1}. \tag{S38}$$

These results match the ones obtained in Ref. [S3], which serves as a confirmation that the methods are powerful (no diagonalisation was needed, for instance).

The authors thank the support from the EU H2020 Quantum Flagship project QMiCS (820505). MC acknowledges support from the DP-PMI and FCT (Portugal) through scholarship PD/BD/135186/2017. MC and YO thank the support from Fundação para a Ciência e a Tecnologia (Portugal), namely through project UIDB/50008/2020, as well as from project TheBlinQC supported by the EU H2020 QuantERA ERA-NET Cofund in Quantum Technologies and by FCT (QuantERA/0001/2017). MS thanks support from the Spanish Government PGC2018-095113-B-I00 (MCIU/AEI/FEDER, UE), and Basque Government IT986-16, the project OpenSuperQ (820363) of the EU Flagship on Quantum Technologies, as well as the EU FET Open project Quromorphic (828826). This work is supported by the U.S. Department of Energy, Office of Science, Office of Advanced Scientific Computing Research (ASCR) quantum algorithm teams program, under field work proposal number ERKJ333.

* mateo.casariego@tecnico.ulisboa.pt
† yasser.omar@lx.it.pt
‡ mikel.sanz@ehu.es

[S1] G. Adesso, S. Ragy, and A. R. Lee. Continuous variable quantum information: Gaussian states and beyond. Open Systems & Information Dynamics, 21(01n02):1440001 (2014).
[S2] D. Šafránek, A. R. Lee, and I. Fuentes. Quantum parameter estimation using multi-mode Gaussian states. New Journal of Physics, 17(7):073016 (2015).
[S3] M. Sanz, U. Las Heras, J. J. García-Ripoll, E. Solano, and R. Di Candia. Quantum estimation methods for quantum illumination. Phys. Rev. Lett., **118**, 7 (2017).